Prefrontal deep projection neurons enable cognitive flexibility via persistent feedback monitoring

Spellman T,[1*], Svei M[1], Liston C[1]

[1]Feil Family Brain and Mind Research Institute, Weill Cornell Medicine, New York, NY 10021

*Corresponding Author
Timothy Spellman, Ph.D.
Instructor in Neuroscience
Weill Cornell Medical College
413 East 69th St, 10th Floor
New York, NY 10021
202-997-1322
tis2013@med.cornell.edu

Acknowledgements
T.S. is supported by NIH (1K99MH117271), the Brain and Behavior Research Institute, and the Leon Levy Foundation. C.L. is supported by NIH (R01 NS095441, MH109685) and by the Rita Allen Foundation.

Abstract

Cognitive flexibility, the ability to alter one's strategy in light of changing stimulus-response-reward relationships, is a critical tool for acquiring and updating learned behavior. In order to adapt to novel, uncertain, or dynamic contexts, it is often necessary to abandon previously successful rules and explore new rules, based on trial and error. One behavioral model of cognitive flexibility, *set-shifting*, entails ignoring a previously relevant stimulus feature in favor of a newly relevant feature. Successful performance on these tasks has been shown to involve the prefrontal cortex (PFC), and impairments in set-shifting are associated with multiple psychiatric disorders. In spite of the translational importance of this behavior, it remains unclear which cell types within PFC are responsible for conveying information critical to set-shifting to downstream regions. To address this question, we developed a novel task for head-fixed mice to test the role of two major PFC projections, the cortico-striatal and cortico-thalamic pathways, in set-shifting behavior. Using optogenetics and 2-photon calcium imaging, we found that these cell types robustly and persistently encoded feedback from the outcomes of recent trials, and that the activity of both cell types during the inter-trial interval was critical to successfully switching between task rules. Moreover, we found that both populations displayed a topological gradient, with neurons located further from the pial surface representing more task-critical information. Together, these findings suggest that deep PFC projection neurons enable set-shifting through monitoring of feedback from recent trials.

Introduction

The ability to rapidly respond to changing external contingencies is critical for any organism that must navigate through a dynamic environment. This *cognitive flexibility* is central to how cognitively advanced organisms learn to interact with the world. A form of cognitive flexibility frequently employed in clinical assessments is *set-shifting*, a kind of task-switching behavior that requires a subject to ignore a previously relevant stimulus feature and instead attend to a previously irrelevant feature to execute a correct response[1,2].

Impairment in set-shifting is a prevalent cognitive symptom in a range of psychiatric disorders[3–7] and often persists despite remission of positive symptoms[8–10]. Prefrontal cortex (PFC) plays a critical and well-established role in supporting set-shifting behavior in human[11,12] and rodent models[13–15], but the circuit elements within PFC that enable set-shifting remain largely unknown. A functional dissection of the prefrontal circuitry underlying set-shifting is of particular translational interest because pharmacotherapeutic interventions in this circuitry can have complex or paradoxical effects by acting on competing circuit elements[16], which may account for the deleterious cognitive side effects that accompany SSRIs and antipsychotics[17,18].

The critical contribution of PFC activity to set-shifting may be mediated by a number of output pathways, but two PFC projection targets of particular interest are the projection to ventromedial striatum (PFC-VMS) and to the medio-dorsal thalamus (PFC-MDT). In rodents, both target structures have established roles in set-shifting behavior[19–22], and PFC projections to both structures underlie behavioral flexibility behavior[23,24].

Neural activity in primate prefrontal cortex has been shown to encode abstract, context or rule-related information[25–27], and in rodents performing set-shifting tasks, such rule-related representations can shift flexibly with repeated changing stimulus-reward contingencies[28,29]. In light of the critical role of PFC in cued modulation of attention[30], the idea that PFC activity might drive the execution of correct responses during set-shifting tasks remains a well-predicated hypothesis.

Alternatively, because set-shifting performance is based on continuous trial-and-error, and rules are not explicitly cued, the role of PFC in set-shifting may be in monitoring feedback. In addition to encoding context, prefrontal activity has been shown to represent feedback signals associated with trial outcome[31,32], and recent evidence suggests that such feedback-related activity is critical for performing task-switching behavior[33,34].

To examine the roles of PFC output neurons in set-shifting performance, we validated a novel set-shifting task for head-fixed mice to enable 2-photon imaging during behavior. Muscimol infusion in PFC impaired performance in both initial and overtrained set-shifting sessions. Shifts were acquired gradually and exhibited characteristic switching costs, and performance depended upon rule-related information from recent trials. Signals for left/right response and trial outcome were decoded from neural population activity only *after* trial completion and persisted for four subsequent trials (up to 55 seconds). Separate analysis of PFC-VMS and PFC-MDT neurons revealed robust representations of all task-related features in both cell types, with strikingly similar trial responsiveness and temporal dynamics. Optogenetic inhibition of either cell type had no effect on performance when delivered *during* trials, but inhibition *following* trials, during the inter-trial interval, impaired performance. Analysis of the topological distribution of response and outcome-selective cells revealed a medial-lateral gradient, with more informative cells located further from the pial surface, indicating a prominent role for projection neurons in deeper cortical layers in conveying feedback-related information to the downstream regions.

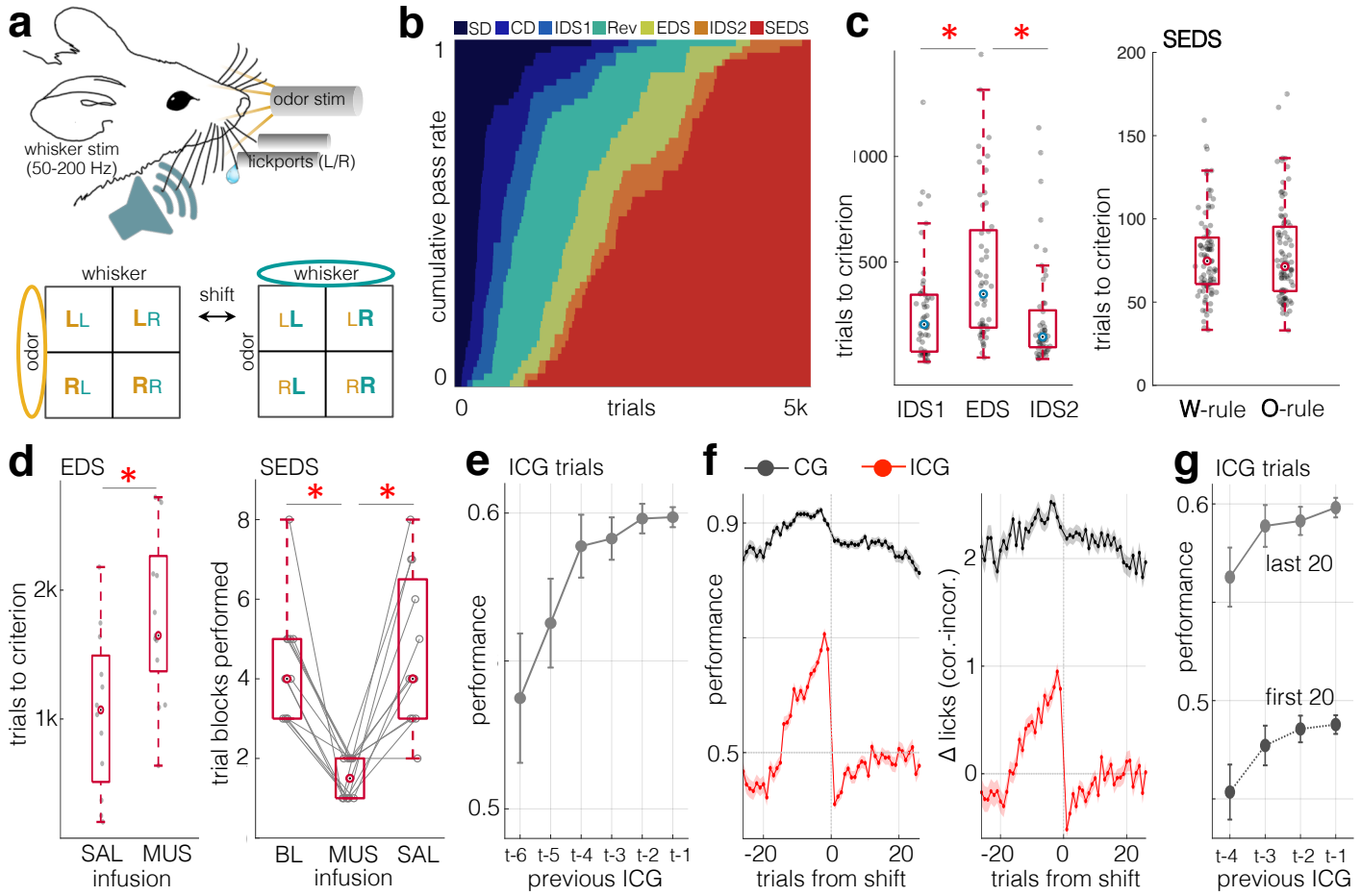

Figure 1

a) Task schematic. Top: diagram of stimulus delivery and lick response setup. Bottom: relevant and irrelevant stimuli and rule shifting.

b) Training curves for seven learning stages. Y-axis denotes the proportion of animals at a given learning stage after trial number x. SD = Simple Discrimination, CD = Compound Discrimination, IDS1 = Intradimensional Shift (initial stimulus modality), Rev = Reversal (initial stimulus modality), EDS = Extradimensional Shift, IDS2 = Intradimensional Shift (second stimulus modality), SEDS = Serial Extradimensional Shifting. N = 53 animals. Trials displayed are concatenated from across multiple sessions (Mode = 350 trials/session).

c) Left: Number of trials to criterion, Intradimensional vs Extradimensional Shift, n = 53 animals, sign rank = 0.0034, 6*10^-5 for IDS1/EDS, IDS2/EDS, 0.2 for IDS1/IDS2. Right: Mean trials to criterion during SEDS, whisker rule vs odor rule. N = 100 animals, signed rank = 0.45.

d) Left: trials to criterion in EDS sessions following transcranial infusion (SAL = saline; MUS = muscimol). N = 12, 13 (SAL, MUS). Rank sum p = 0.02. Right: Number of trial blocks reaching criterion performance in SEDS sessions following 10 rule shifts. N = 12; median blocks (BL/MUS/SAL): 4, 1.5, 4. Sign rank p = 0.0005 (BL/MUS), 0.001 (SAL/MUS), 0.68 (BL/SAL). Median total trials completed: SAL = 644; MUS = 651; sign rank p = 0.52.

e) Incongruent trial performance by recency of previous incongruent trial during SEDS sessions (mean ± SEM). N = 2681 shifts, 100 animals.

f) SEDS trial performance relative to rule shift (CG = congruent, ICG = incongruent). Left: proportion of trials correct. Right: anticipatory licking (correct – incorrect direction). N = 2681 shifts in 100 animals.

g) Incongruent trial performance by recency of previous incongruent trial during first 20 and last 20 relative to rule shift (mean ± SEM). Same animals and sessions as **f**.

A cross-modal set-shifting task for head-fixed mice

To image set-shifting behavior in mice, a head-fixed paradigm leveraging the sensitivity of olfactory and whisker somatosensory systems was developed. Water-restricted mice were presented on each trial with one of two possible whisker stimuli and two possible odor stimuli, in randomized combinations, with left and right lickspouts serving as behavioral readouts. Animals underwent a standardized series of transitions in task structure (Fig. 1 and Methods), culminating in a Serial Extradimensional Shifting task (SEDS), in which the relevant modality switched upon reaching a criterion performance of 80% correct within a 30-trial moving window. Animals took longer to perform an extradimensional shift (EDS) between modalities than to acquire a new set of exemplars within either modality (Fig. 1c), and there was no difference between modalities in trials to criterion

(Fig. 1c). Infusion of muscimol within PFC increased trials to criterion in the initial EDS shift, as well as after completing 10 shifts of SEDS (Fig. 1d), indicating that set-shifting in this paradigm is dependent on PFC activity, both initially and after repeated shifts.

Trials belonged to two classes: those in which whisker and odor stimuli would indicate the same response direction (*congruent* trials), and those in which the two stimuli would indicate opposing directions (*incongruent* trials). Incongruent trials alone, therefore, required application of the modality rule, and feedback from incongruent trials carried information about modality rule. Animals used prior incongruent trial information to guide behavior, as performance on incongruent trials declined with the number of intervening congruent trials since the most recent incongruent trial (Fig. 1e). This held true in trials occurring both early and late within trial blocks (Fig. 1g). Performance on incongruent trials dropped below chance following rule switches, revealing perseverance of the previous rule (Fig. 1f). Sub-chance performance persisted over multiple incongruent trials, following a gradual reversion to chance performance before new rule new rule was acquired (Fig. 1f).

PFC population activity persistently represents trial feedback information

To assess task-related activity in PFC neurons, GCaMP6f-mediated 2-photon calcium imaging was performed through a coronally-implanted microprism, allowing for a field of view that preserved cortical laminar structure and included both prelimbic and infralimbic areas (Fig. 2a). Analysis of task responsiveness across learning stages revealed that, while signal corresponding with the relevant stimulus was present from the earliest recorded session (CD) and remained throughout all subsequent task stages, signal corresponding with the irrelevant stimulus emerged only after the EDS session (Fig. 2c). While few neurons were modulated by trial outcome in early sessions, outcome-modulated responses emerged over the course of multiple task transitions (Fig. 2c). Analysis of SEDS sessions with maximum-margin linear decoders revealed robust representations of whisker and odor stimuli, response, trial outcome, and task rule (Fig. 2e).

Because response and cue direction were potentially highly correlated features of the neural activity, decoders were next trained and tested across trial outcome (trained on correct trials and tested on incorrect trials, and vice versa). When applied to recordings from initial CD sessions, this procedure revealed a significantly *below chance* decoder performance, indicating that the neural population signal was dominated by cue representation and that no independent response representation was measured. When applied to recordings from SEDS sessions, an independent response representation emerged *following* the behavioral response. Population signal, therefore, bore robust representation of the already selected response direction and did not explicitly predict response direction prior to the time of selection (Fig. 2f). The same approach was used to decode trial outcome across response directions, revealing a robust signal for outcome that emerged only after termination of the trial.

Response and outcome, but not cue direction (or whisker or odor stimulus) could be decoded with better than chance success from up to four trials in the past (Fig. 2g). Importantly, as a control for autocorrelation of the behavior and/or neural activity, none of these features could be decoded from future trials.

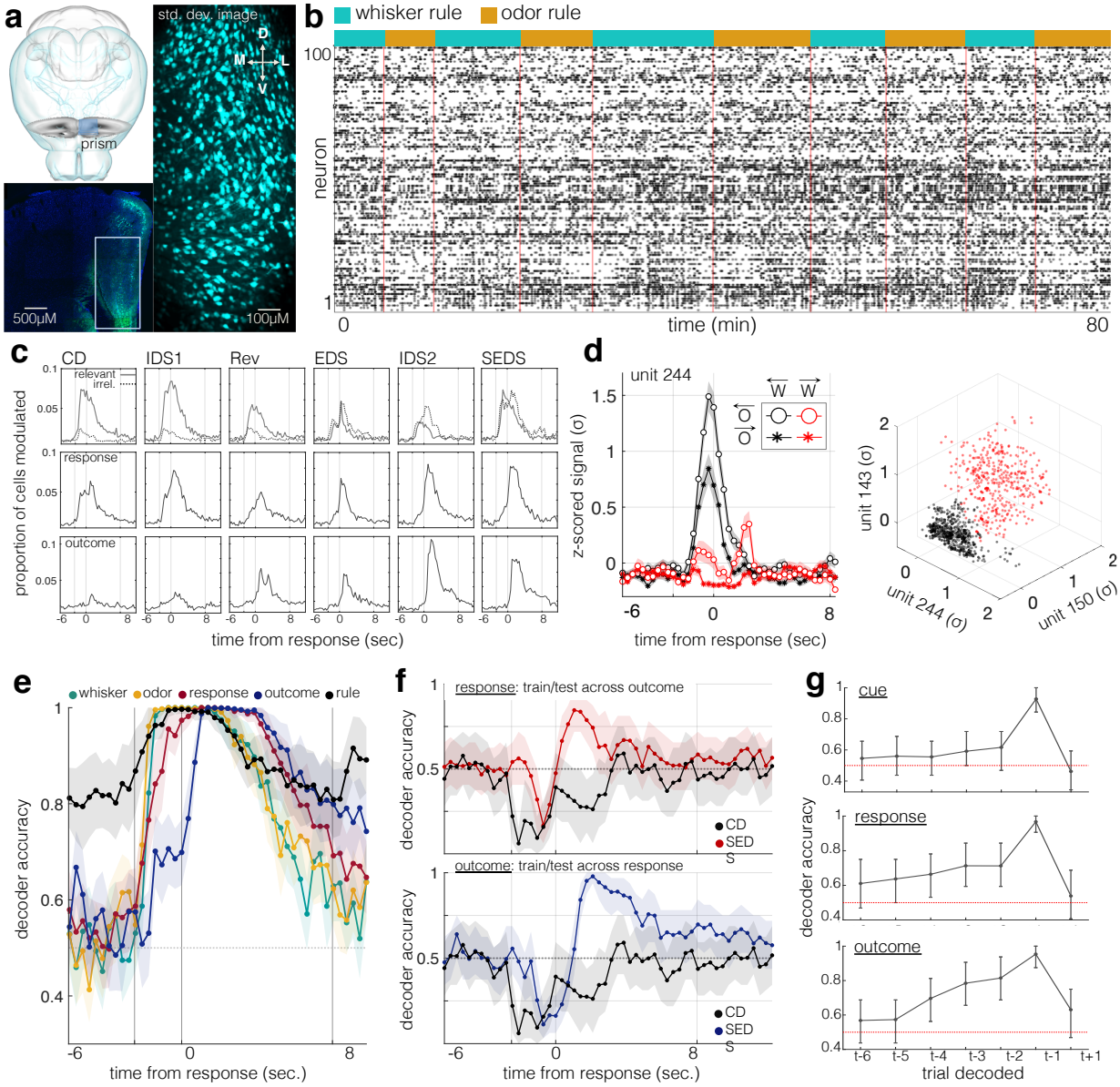

Figure 2

a) Top left: schematic of coronal prism implantation field. Bottom left: hSyn-GCaMP6f fluorescence in fixed tissue (DAPI in blue). Right: standard deviation image from 115-min. hSyn-GCaMP6f recording (~3Hz, N = 953 extracted units). Note: different animal from bottom left.

b) Top: thresholded/rasterized events from deconvolved calcium traces. N=100 units recorded over the course of 10 trial blocks.

c) Histograms: proportion of cells modulated by task features over trial-aligned timepoints and through learning stages. Stimulus presented from -2.5s (first tick mark) to 0s (second tick mark). Response window is 0s - 1.5s. Subsequent trial onset ≥8s. Top row: stimuli. Solid: initially relevant stimulus; dashed: initially irrelevant stimulus. Middle row: response direction. Bottom row: trial outcome.

d) Left: mean ± SEM of z-scored traces from example units during trials with four stimulus combinations. Right: trial-separated z-scores for left/right whisker stimuli in a 3-unit space.

e) SVM decoder accuracy for five task-related features, temporally aligned to the response window.

f) Top: SVM decoder accuracy for response tested across outcomes (gray: CD; red: SEDS). Bottom: SVM accuracy for outcome tested across responses (gray: CD; red: SEDS).

g) Means ± 95% confidence intervals for decoders tested on past (t-...) and future (t+...) trial features. Top: cue direction. Middle: response direction. Bottom: trial outcome. Red dashes: chance performance.

Similar task responsiveness in two major PFC projection neuron populations

Analysis was next focused on PFC-VMS and PFC-MDT populations. Labeling of both populations within the same animals revealed the two cell types to be spatially intermingled, with PFC-VMS neurons largely present in layers II/III and V, and PFC-MDT neurons largely present in layer V (Fig. 3b). Despite their being spatially interspersed, the two populations showed little (<5%) overlap (Fig. 3b), indicating two distinct projection populations. The two populations showed similar responsiveness to task features, both robustly representing trial response and outcome with similar time courses (Fig. 3c). Similar proportions of neurons within each type also showed excitation and inhibition with stimulus onset (Fig. 3d), and similar proportions of individual units from the two projections showed modulation by trial response and outcome, with parallel emergence through distinct learning stages (Fig. 3e).

The finding of persistent representation of trial feedback signals raised the possibility that the task-critical role of the PFC might be feedback monitoring. The similar physiological task responsiveness of the two projection populations suggested that both cell types might critically support set-shifting performance by enabling feedback monitoring during the inter-trial interval. We next tested this hypothesis using projection-targeted optogenetics.

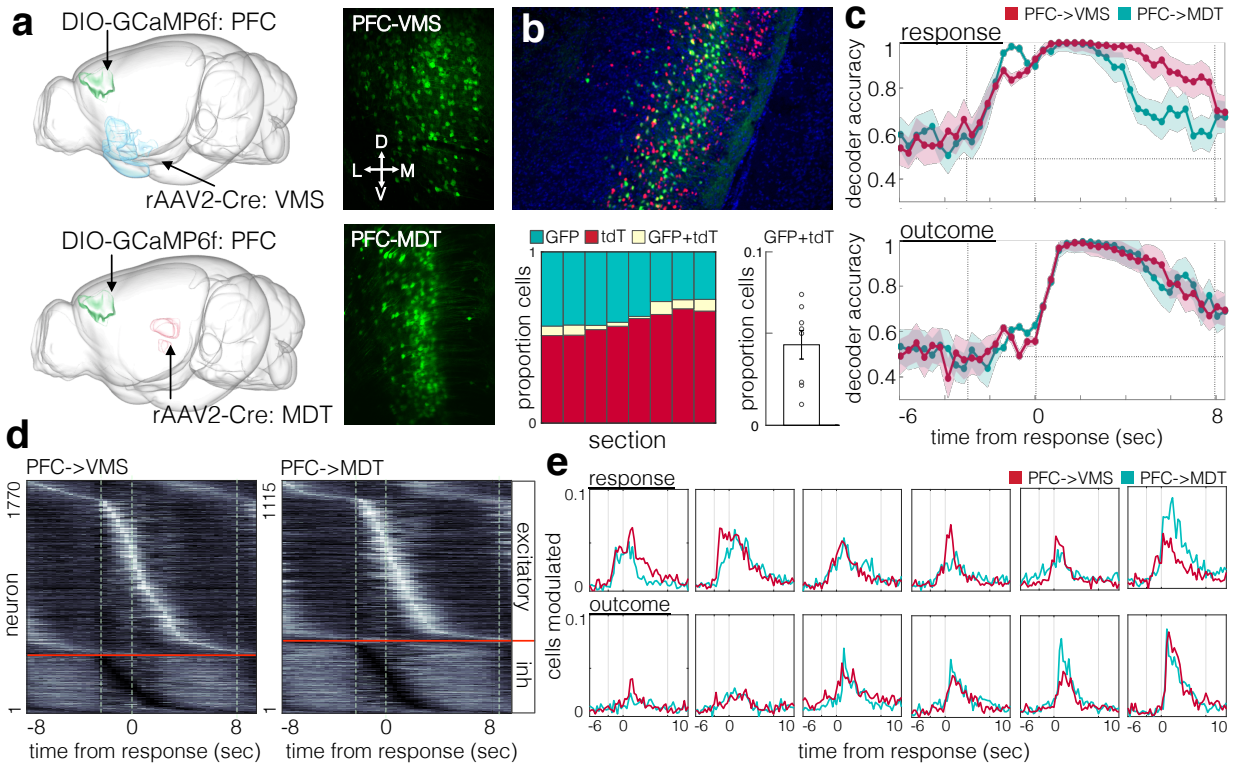

Figure 3

a) Dual projection neuron labeling approach. Top: PFC->VMS neurons. Bottom: PFC->MDT neurons. Left: viral targeting. Right: GCaMP6f in projection-specific neural populations.

b) Dual PFC->VMS and PFC->MDT projection labeling in a single brain. Top: green is rAAV2-CAG-mNeuroGFP in MDT; red is AAV1-hSyn-DIO-nls-tdTomato in PFC and CAV2-Cre in VMS (DAPI in blue). Bottom left: relative green, red, and overlapping cell counts. Bottom right: median relative overlap (N = 8 sections, 2 animals, mean=4.6±0.8%).

c) SVM decoder accuracy for response (top) and outcome (bottom) across trial-aligned timepoints for PFC->VMS (red) and PFC->MDT populations (green). Stimulus onset = -2.5s (first vertical dash). Response window is 0s-1.5s. Subsequent trial ≥8s. N=1770 units (PFC->VMS) and 1115 units (PFC->MDT).

d) Trial-averaged histograms for same PFC->VMS (left) and PFC->MDT (right) units as in c. Rows are z-scored traces, normalized to trial-aligned absolute maxima.

e) Histograms: proportion of cells modulated by task features over trial-aligned timepoints and through learning stages for PFC->VMS (red) and PFC->MDT (green) units. Stimulus presented from -2.5s (first tick mark) to 0s (second tick mark). Response window is 0s - 1.5s. Subsequent trial onset ≥8s. Top row: response direction. Bottom row: trial outcome.

Interference with feedback monitoring in PFC projection populations impairs set-shifting

We used a soma-targeted anion-conducting channelrhodopsin (stGtACR2)[35] to inhibit PFC activity during set-shifting in one of three temporally-controlled regimes (Fig. 4a). Photoactivating light stimulation was delivered during trials (0.5s trial-ready cue period, 2.5s stimulus presentation, and ≤1.5s response window), or during inter-trial intervals (8-10s epoch triggered on response lick) following congruent or incongruent trials (Fig. 4b). Trial blocks alternated light on/off. Photoactivation of pan-neuronally-expressed stGtACR2 during the inter-trial interval following incongruent trials impaired performance on incongruent trials (Fig. 4c) but not on congruent trials (Fig. 4d). This effect was also seen in animals expressing stGtACR2 in PFC-VMS and PFC-MDT projection neurons (Fig. 4c-d). No impairment was seen on incongruent trial performance for either projection population when light was delivered following congruent trials (Fig. 4e), indicating that the impairment seen with post-incongruent inhibition reflected an interference with prior trial feedback, rather than preparation for the subsequent trials. Neither PFC-VMS nor PFC-MDT activity was necessary for execution of the rule-guided response, as no impairment was seen with photoactivation during incongruent trials (Fig. 4f). Together, these results indicate a parallel, critical role for both PFC projection populations in monitoring the outcomes of the rule-informative incongruent trials, a function which is selectively important for subsequent incongruent trials.

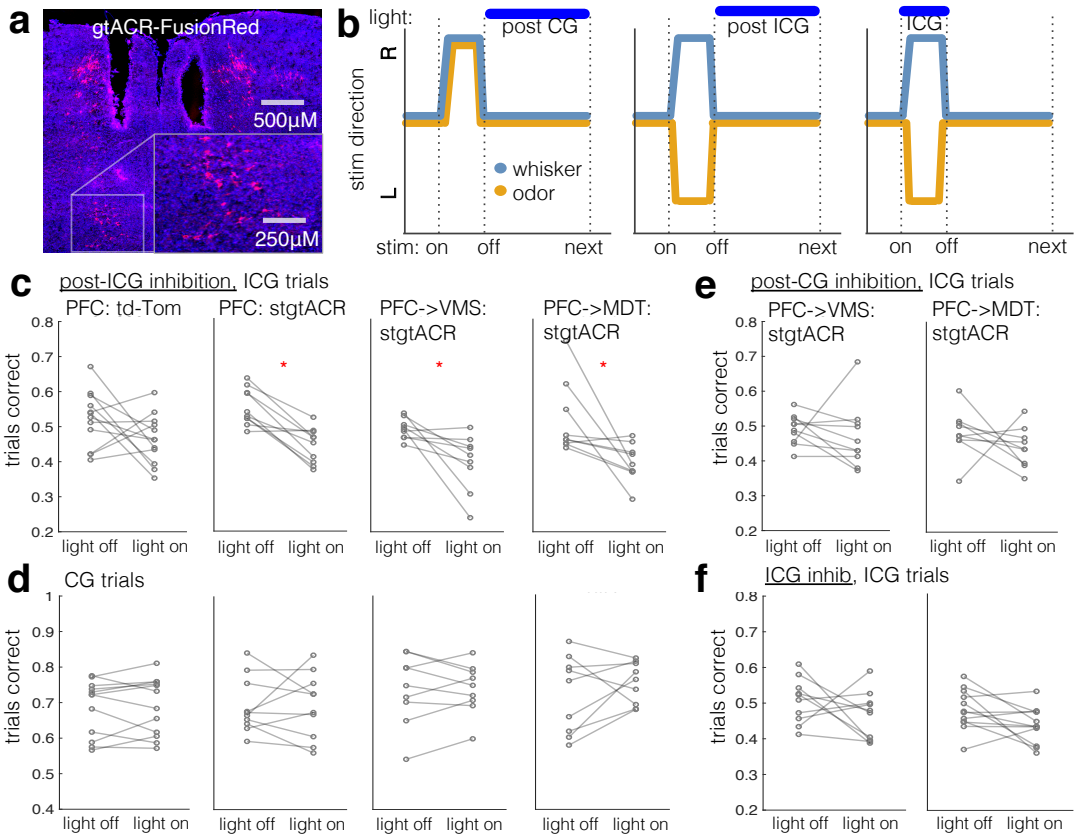

Figure 4

a) Cre-mediated expression of gtACR-FusionRed in PFC->VMS neurons, and fiber tracks from chronically implanted bilateral optical fibers (fixed dissue, DAPI in blue).

b) Schematic of light delivery conditions.

c) Effect of light stimulation following incongruent trials on incongruent trial performance (proportion of trials correct). Left: viral control animals (td-Tomato expressed in PFC); second from left: animals with pan-neuronal expression of stgtACR in PFC; third from left: animals with stgtACR expressed in PFC->VMS projection neurons; right: animals with stgtACR expressed in PFC->MDT projection neurons. N = 12, 10, 9, 9, resp. Sign rank p = 0.20, 0.004, 0.012, 0.012, resp.

d) Effect of light stimulation during ITIs following congruent trials on incongruent trial performance. N = 9, 9, resp. Sign rank p = 0.19 and 0.16, resp.

e) Effect of light stimulation during ITIs following congruent trials on incongruent trial performance. N = 9, 9, resp. Sign rank p = 0.19 and 0.16, resp. Effect of light stimulation during ITIs following incongruent trials on congruent trial performance (proportion of trials correct). Left to right: as in (a) above. N = 12, 10, 9, 9, resp. Sign rank p = 0.85, 0.69, 0.91, 0.30, resp.

f) Effect of light stimulation during trials (stimulus presentation + response window) on incongruent trial performance. N = 12 and 12, resp. Sign rank p = 0.32 and 0.11, resp.

Feedback-related activity follows an anatomical gradient independent of projection subtype.

The striking similarity of both task-related activity and the task-critical function of the PFC-VMS and PFC-MDT pathways left open the question of whether any common spatial/anatomical organization is shared between the two populations. We therefore examined whether the relative locations of neurons within the PFC imaging field affected task-related activity. As demonstrated in sensory cortex[36], temporal correlations across pairs of simultaneously-recorded neurons decay with distance (Fig. 5a), demonstrating an association between anatomical location and temporal activation within the context of the task. More deeply located neurons (further from pial surface) showed greater magnitude of trial-induced responses, and trial-averaged traces showed greater variance at deep locations (Fig. 2b); this included neurons both activated and inhibited by trial onset. Increased response magnitude was seen in deeper neurons from both projection populations, and with similar spatial correlation (Fig. 2d). In addition to greater trial responsiveness, task-related information was heterogeneously distributed across the cortical laminar axis, with more deeply located neurons contributing greater β-weights to linear decoders for response and outcome during the inter-trial interval (Fig. 5e). General linear models for the β-weights of response and outcome yielded significant coefficients for neuron depth but not for projection type. Confirming the differential contribution of neurons from deep and superficial areas to decoder accuracy, binned subpopulations from spatial quartiles showed differential accuracies, with decoders comprised of deeper neurons showing greater accuracy for response and outcome during the ITI than those comprised of more superficial neurons (Fig. 5f).

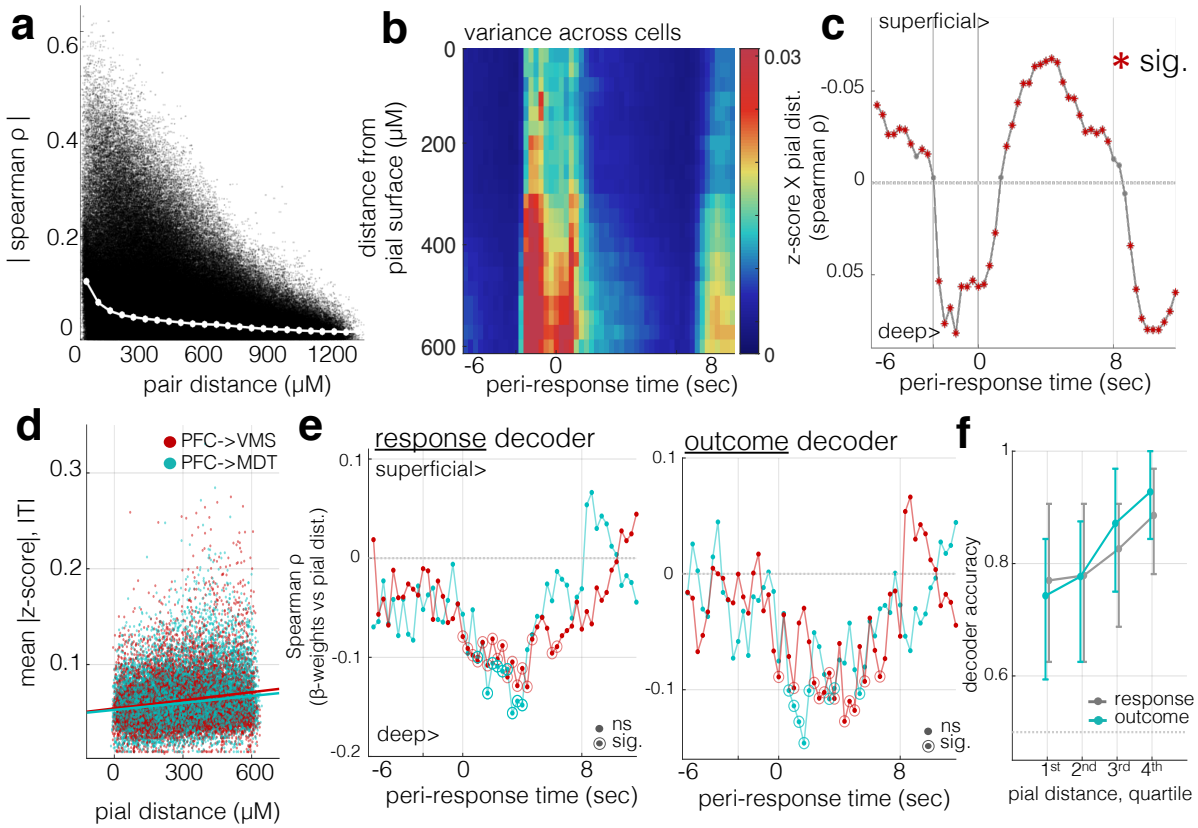

Figure 5

a) Spatial distance of simultaneously recorded unit pairs vs. temporal correlation (N = 1562607 pairs from 4740 units in 21 animals). White = mean ± SEM, 50μM bins.

b) Cross-unit variance of trial-averaged activity, over trial-aligned timepoints and relative distance from pial surface. Warmer colors correspond with higher cross-unit variance per spatiotemporal bin. Units are z-scores. Same 4740 units as in a.

c) Correlation of unit population activity by pial distance over trial-aligned timepoints. Asterisks are significant for Bonferoni-corrected rank sum scores.

d) Correlation of absolute values of unit z-scored activity with relative pial distance during ITI for PFC->VMS and PFC->MDT neurons. PFC->VMS Spearman ρ = 0.16, p = 8e-79, 1770 neurons, 9 animals; PFC->MDT Spearman ρ = 0.12, p = 3e-52, n=1155 neurons, 8 animals.

e) Correlations of SVM β-weights with pial distance at trial-aligned timepoints. Larger circles, Spearman p<0.01. PFC->VMS red, PFC->MDT green (same units as in d).

f) Mean ± 95% confidence intervals for response and outcome decoders by relative pial distance quartiles. Same cells as d-e.

Discussion

We combined projection-targeted *in vivo* calcium imaging with optogenetics to identify the relative contributions of two major PFC projection subtypes to a validated behavioral model of cognitive flexibility in mice. We found that PFC activity persistently tracked recent trial histories, sustaining representations of response and outcome, but not stimulus identity or cue direction, over multiple trials. The behavioral importance of these feedback signals was confirmed by temporally precise inhibition, which revealed that PFC activity following the rule-informative incongruent trials, but not following the uninformative congruent trials, impaired behavior, and that neither population was critical to the execution of rule-dependent responses in real-time. PFC-VMS and PFC-MDT projections played parallel roles in the task, exhibiting similar, task-critical activity, and both contributed to a spatial functional gradient, with more deeply located neurons in both groups displaying more task-critical information during the feedback epoch.

While the primary motivation behind the development of this task was to functionally emulate clinical assessments of cognitive flexibility, there is also an extensive literature within human psychology that concerns task-switching and the study of switching costs[37]. Indeed, we note that, as with previous rodent behavioral models of task-switching[38], mice here exhibit switching costs that persist well beyond the first trial (Fig. 1f), that they appear to use model-free learning, and that this differentiates them from their human counterparts. We also note our use of the term *serial extradimensional set-shifting*, where the term *task switching* is more often used to refer to paradigms with multiple, bidirectional changes in stimulus-response-reward contingencies. We do so to differentiate from the reversal, intradimentional, and first-time extradimensional transitions, which here form distinct learning stages and which are also forms of task-switching. Nevertheless, increased trials to criterion for extradimensional vs. intradimensional shifts (Fig. 1c) and elevated reaction times on incongruent vs. congruent trials[39] are hallmarks of shifting across feature dimensions.

While the finding of a critical role for PFC output neurons in supporting feedback monitoring in set-shifting was in keeping with the initial hypothesis, the lack of behavioral impairment seen when inhibiting these pathways during trials was striking, particularly given the robust activation of stimulus-selective representations seen across PFC activity during the stimulus presentation and response selection epoch. The observation of strong task-related activity, which is nevertheless evidently not task-critical, leaves unanswered the question of what adaptive purpose this activity may serve and reinforces the need to assess the role of neural signals through modulation, rather than assuming a critical role for observed activity.

The PFC-MDT population targeted in these experiments is confined largely to layer V. This distinguishes it from layer VI cortico-thalamic neurons, also found in PFC and elsewhere in cortex. It should be noted that these projections were labeled using a rAAV2 vector, which has selective tropism for layer V PFC-MDT neurons, rather than canine adenovirus (Cav2), which preferentially infects axons of layer VI neurons[40]. This differential labeling, along with pronounced task differences, may account for differential effects of projection neuron inhibition relative to other PFC projection targeting studies[41].

Feedback signals within PFC are modulated by expectation and by cognitive states, including attention[42]. Extensive research in feedback-related negativity[43] and reward prediction error[44] support the idea that feedback-related signals in prefrontal areas are dynamically mediated by ongoing task demands and are disrupted in disorders in which set-shifting is also disrupted[45]. The overt behavior performed in the compound discrimination task is identical to that performed during set-shifting: the animal is presented with cues comprised of two stimulus modalities and responds to one with a left or right lick. The fact that dedicated response and outcome signals are absent during early compound discrimination sessions and emerge as changing task rules require inferential learning, (Fig. 2 c,f) provides strong support for the idea that these signals are not innate but are brought about by the demands of feedback monitoring. Future work will attempt to elucidate the mechanisms behind these signals, which may depend upon neuromodulatory input.

Methods

Subjects

Male C57BL/6 mice (Jackson Labs) were used for all experiments, aged 6-10 weeks at first use. Mice were housed in a Weill Cornell Medical College facility and were maintained on a 12-hour light-dark cycle. Except when water-restricted for the purpose of behavioral training and testing, all mice were given *ad libitum* access to food and water. Littermates underwent prism or fiber implant surgeries typically within the same week, so mice were group-housed with littermates with the same implantation status. All procedures were approved by the Weill Cornell Medicine IACUC. Sample sizes for each experiment were determined using power analysis estimates computed in Matlab, based on anticipated effect sizes that were estimated from previously published reports whenever they were available, and were powered to detect moderate, biologically meaningful effect sizes.

Surgery

Animals were placed inside a flow box and anesthetized with isoflurane gas (2%) until sedated, at which point they were placed in a stereotax and maintained on 0.5% isoflurane for the duration of the surgery. Scalp hair was trimmed away, and a midline incision was made using fine surgical scissors (Fine Science Tools), exposing the skull. The periosteum was bluntly dissected away and bupivacaine (0.05 mL, 5 mg/kg) was topically applied. For prism implantation, a large rectangular craniotomy was made above left PFC, extending from 1.5mm anterior to 3.7mm anterior, and from 2.0mm lateral (left) to 0.2mm lateral (right, across midline).

A 0.5-mm burr (Fine Science Tools) and a high-speed hand dental drill (Osada) were used, taking great care not to compress brain tissue or damage the sagittal venous sinus. Gentle irrigation with phosphate-buffered saline (137 mM NaCl, 27 mM KCl, 10 mM phosphate buffer, VWR) was used to clear debris at regular intervals. The dura beneath the craniotomy was removed using fine forceps (Fine Science Tools).

Chronically implanted microprisms were 1.5mm X 1.5mm X 3mm microprism (M/L,A/P,D/V) from OptoSigma (BK7 borosilicate glass with aluminum hypotenuse and silicon dioxide coating), which was implanted at a depth of 2.3mm ventral to brain surface using a stereotaxic micromanipulator (Kopf), with the prims held in place using vacuum suction via an 18G blunt needle. Minimal reactive gliosis was seen in the coronal imaging field, and maximum calcium-mediated fluorescence was seen 50-150μM past the prism face, and therefore imaging planes were confined to this depth.

For PFC-VMS and PFC-MDT projection targeting, additional craniotomies were made at 1.25mm/1.25mm A/L and 1.2mm/0.35mm P/L, respectively. All head-fixed animals received custom-machines stainless steel head plates affixed with Metabond dental cement. Head plates featured a circular central aperture centered around the imaging field (9mm I.D.), with right and left arms securing (25mm total width) that accommodated 0-80 socket screws (0.38g in total). Sterile eye lubricant (Puralube, FischerSci) was administered to prevent corneal drying, and a microwavable heating pad (Snugglesafe) was used to maintain body temperature. Metacam (1 mg/kg, i.p.) was administered after surgery as a prophylactic analgesic.

Viral Transduction

AAV1 of titer exceeding 10^{12}vg/ml (Vector Biolabs, UNC Vector Core and Addgene) was used to package the plasmids. For imaging experiments, AAV1-hSyn-GCaMP6f or AAV1-hSyn-DIO-GCaMP6f was targeted to PFC. Injection coordinates for PFC were 1.75mm anterior. Two parallel injection tracks were made at 0.2mm and 0.5mm lateral, and in each of these tracks, two D/V sites received infusions, at 2.0mm and 1.5mm ventral to brain surface. For rAAV2-Cre projection targeting, VMS injections were delivered at 1.25mm/1.25mm/4.7mm A/L/V, and MDT injections at 1.2mm/0.35mm/3.2mm P/L/V. Hamilton syringes and beveled 36G or 33G NanoFil needles (WPI) were used, and at each site, the needle was allowed to sit 5min to allow for tissue settling before infusion. Virus was infused at a rate of 50nL/min, for a total of 250nL per site.

For the dual labeling tracing experiment, rAAV2-mNeuroGFP was injected in MDT (500nL), rAAV2-Cre was injected in VMS (500nL), and AAV1-NLS-tdTomato was injected in PFC (500nL).

Optogenetic implantation and stimulation

Bilateral fibers were implanted over PFC (Thorlabs dual fiber cannulae, 700μM center-to-center spacing, 200μM core) at 0.35mm lateral, 1.75 anterior, 1.2mm ventral to brain surface. Light was delivered via Thorlabs M470F3 fiber-coupled LED, 1.5-3mW light power from each fiber. In the trial stimulation condition,

photoactivation was initiated concurrently with the 500ms trial-ready cue and persisted through the 2.5s stimulus presentation epoch until either a lick terminated the trial or the 1.5s response period expired. In the inter-trial interval stimulation conditions, photoactivation was initiated concurrently with lickspout selection and persisted through the 8-10s post-trial epoch, terminating with the onset of the following trial-ready cue.

2-photon imaging

Imaging was performed via custom-designed Objective was 10x 0.6NA Olympus, with 8mm working distance. All images were acquired using a commercial two- photon laser-scanning microscope (Olympus RS) equipped with a scanning galvanometer and a Spectra-Physics Mai Tai DeepSee laser tuned to 920nm. Fluorescence was recorded through gallium arsenide phosphide (GaAsP) detectors using the Fluoview acquisition software (Olympus) using a green light emission bandpass filter (Semrock). All imaging experiments began by obtaining an isosbestic anatomical scan (810nm 2P excitation light) to aid in relocating the same sites over multiple sessions. Calcium signals were acquired at 256 X 130 pixel resolution, covering a 1500μM X 760μM field of view, for a μM/pixel ratio of 5.85, and the scan time was 346ms, for a frame rate of 2.89Hz. All calcium imaging experiments occurred in awake mice.

Image processing

Videos were motion-corrected using NoRMCorre[46] in Matlab (Mathworks), and a constrained non-negative matrix factorization-based source extraction methods was used to denoise, deconvolve and demix the videos to produce neural traces (CNMFE package[47]). The resulting traces were deconvolved calcium traces corresponding with estimated event rates, which were then z-scored over the full session to normalize. Calcium signals from sequential sessions were concatenated using CellReg[48].

Behavioral training and testing protocols

Animals recovered 14 days from surgery before being placed on water restriction, after which time they received 1.2mL/day. Animals underwent two days of hand-feeding, in which they were handled for up to ten minutes by the experimenter while receiving water from a 1mL syringe with a rounded stainless steel gavage needle. The following day they underwent a Habituation-1 session in the behavioral apparatus, which consisted of an aluminum restraint tube with dual lickspouts positioned at one end. This tube was 27mm in diameter, a width calibrated to allow the animal to groom and adjust its posture during sessions but which prevented significant lateral or vertical body movement. During Habituation-1, lickspouts were alternately armed so that a single lick would trigger delivery of a 3uL water bolus, and the identity of the armed lickspout changed every 1-3 licks, with a 1.5s timeout after each bolus delivery. This alternating schedule forced the animal to explore both lickspouts equally to maximize rewards. Animals would periodically venture out of the restraint tube to explore the behavior chamber, at which point the experimenter would guide them back into the tube. The session terminated when the animal reached satiety, and the animal was considered to have passed this stage when it had consumed 500μL in a session. The Habituation-2 stage consisted of the same lick/dispense schedule, but during this session the animal was head-restrained for the first time. Here again, the animal needed to consume 500μL to pass. After this stage animals underwent Habituation-3, in which lickspouts alternated every 20 lick/delivery trials, to establish left/right trial blocks.

After this, animals underwent a Shaping-1 session, which introduced the trial structure to be used for the rest of the sessions: a 500ms white noise trial-start cue was presented, followed by a 2.5s stimulus (whisker or odor, depending on the training sequence, which was counter-balanced across animals), followed by a 1.5s response window, during which the correct lickspout was armed. When the response rate fell to between 0.3 and 0.6 within a 10-trial moving window, reward would be dispensed regardless of whether the animal licked. Trials were blocked (20 right, 20 left), and a lick to the incorrect side would not terminate the trial (the animal as allowed to continue until it licked the correct spout). Criterion for passing Shaping-1 was 500μL consumed. Shaping-2 differed from Shaping-1 in that trials were randomized between sides rather than blocked. Criterion here, and for all remaining sessions up to SEDS, entailed reaching 80% correct within a 30-trial moving window, and simultaneously performing above 50% on both left and right trials, at any point within the session. Following this session, animals underwent Simple Discrimination, in which a lick to the wrong side during the response window would terminate the trial. After reaching criterion, animals underwent Compound Discrimination (CD), Intradimensional Shift-1 (IDS1), Reversal (Rev), Extradimensional Shift (EDS), Intradimensional Shift-2 (IDS2),

and finally Serial Extradimensional Shifting (SEDS). Behavioral data was sent from an Arduino board to a desktop computer through serial input and logged as rich text format files.

Whisker stimulus pairs consisted of either 35Hz vs. 155Hz pure tones, or a 210Hz tone vs. a Poisson click train, all delivered bilaterally. Odor cue pairs consisted of sesame oil vs. olive oil, or almond oil vs. orange extract. Clean air flowed through the odor presentation port (0.2L/min through 1/32" Teflon tubing), and clean air was completely replaced by air channeled through odorant bottles within 50ms from stimulus onset.

Linear decoding with SVM

Population decoding was performed with maximum-margin linear decoders (Matlab fitcsvm). At each iteration data were separated into equally sized training and testing sets, and in each set, trials were separated into equal numbers from each binary value for the feature of interest. To combine inputs from neurons across multiple sessions, and to remove inter-trial variability each of these trial groups was than randomly separated into 16 trial groups, each of which was averaged into one *supertrial* to serve as a decoder input (16 supertrials for one value of the feature of interest and 16 from the opposing value). This number was calibrated to ensure robust trial subsampling within training and testing sets while removing sufficient trial variability to reveal accurate decoding. Confidence intervals were obtained by iterating over 500 subsamplings and identifying centiles. Decoder accuracies performed on data from inter-trial intervals were run on binned activity values over the 4-8 second post response epoch unless otherwise specified.

Muscimol silencing

Animals received chronically implanted 26G bilateral stainless steel guide cannulae (Plastics One), implanted at 1.75mm/0.35mm/1mm A/L/V. After undergoing the training and task transition sequence up to and including Reversal, animals underwent muscimol infusion. In a familiar cage, bilateral internal infusion cannulae were inserted into the guide cannulae, protruding 0.5mm from the end of the guide cannulae, and were left for 5min to allow tissue to settle. Muscimol (1μg/μL) or physiological saline (0.9%) was infused at a rate of 50nL/min, for a total of 0.25μL. Five minutes after completion of the infusion, the internal cannulae were removed and them mouse underwent behavior al testing.

References

1. Heisler, J. M. *et al.* The Attentional Set Shifting Task: A Measure of Cognitive Flexibility in Mice. *J. Vis. Exp. JoVE* (2015) doi:10.3791/51944.
2. Tait, D. S., Chase, E. A. & Brown, V. J. Attentional set-shifting in rodents: a review of behavioural methods and pharmacological results. *Curr. Pharm. Des.* **20**, 5046–5059 (2014).
3. Ceaser, A. *et al.* Set-shifting ability and schizophrenia: a marker of clinical illness or an intermediate phenotype? *Biol Psychiatry* **64**, 782–8 (2008).
4. Jazbec, S. *et al.* Intra-dimensional/extra-dimensional set-shifting performance in schizophrenia: Impact of distractors. *Schizophr. Res.* **89**, 339–349 (2007).
5. Halleland, H., Haavik, J. & Lundervold, A. Set-shifting in adults with ADHD. *J Int Neuropsychol Soc* **18**, 728–737 (2012).
6. Murphy, F. C., Michael, A. & Sahakian, B. J. Emotion modulates cognitive flexibility in patients with major depression. *Psychol. Med.* **42**, 1373–1382 (2012).
7. Disner, S. G., Beevers, C. G., Haigh, E. A. P. & Beck, A. T. Neural mechanisms of the cognitive model of depression. *Nat. Rev. Neurosci.* **12**, 467–477 (2011).
8. Gonda, X. *et al.* The role of cognitive dysfunction in the symptoms and remission from depression. *Ann. Gen. Psychiatry* **14**, 27 (2015).
9. Bortolato, B. *et al.* Cognitive remission: a novel objective for the treatment of major depression? *BMC Med.* **14, Article number: 9**, (2016).
10. Harvey, P., Green, M., Keefe, R. & Velligan, D. Cognitive Functioning in Schizophrenia: A Consensus Statement on Its Role in the Definition and Evaluation of Effective Treatments for the Illness. *J. Clin. Psychiatry* **65**, 361–372 (2004).

11. Milner, B. Effects of different brain lesions on card sorting: The role of the frontal lobes. *Arch. Neurol.* **9**, 100–110 (1963).
12. Kim, C., Cilles, S. E., Johnson, N. F. & Gold, B. T. Domain General and Domain Preferential Brain Regions Associated with Different Types of Task Switching: A Meta-Analysis. *Hum. Brain Mapp.* **33**, 130–142 (2012).
13. Bissonette, G., Powell, E. & Roesch, M. Neural structures underlying set-shifting: roles of medial prefrontal cortex and anterior cingulate cortex. *Behav. Brain Res.* **250**, 91–101 (2013).
14. Birrell, J. & Brown, V. Medial frontal cortex mediates perceptual attentional set shifting in the rat. *J. Neurosci.* **20**, 4320–4 (2000).
15. Brigman, J., Bussey, T., Saksida, L. & Rothblat, L. Discrimination of multidimensional visual stimuli by mice: intra- and extradimensional set shifts. *Behav. Neurosci.* **119**, 839–842 (2005).
16. Miller, P. Dynamical systems, attractors, and neural circuits. *F1000Research* **5**, (2016).
17. Sayyah, M., Eslami, K., AlaiShehni, S. & Kouti, L. Cognitive Function before and during Treatment with Selective Serotonin Reuptake Inhibitors in Patients with Depression or Obsessive-Compulsive Disorder. *Psychiatry J.* **2016**, (2016).
18. Hill, S. K., Bishop, J. R., Palumbo, D. & Sweeney, J. A. Effect of second-generation antipsychotics on cognition: current issues and future challenges. *Expert Rev. Neurother.* **10**, 43–57 (2010).
19. Aoki, S., Liu, A. W., Zucca, A., Zucca, S. & Wickens, J. R. Role of Striatal Cholinergic Interneurons in Set-Shifting in the Rat. *J. Neurosci.* **35**, 9424–9431 (2015).
20. Floresco, S., Ghods-Sharifi, S., Vexelman, C. & O, M. Dissociable Roles for the Nucleus Accumbens Core and Shell in Regulating Set Shifting. *J. Neurosci.* **26**, 2449–2457 (2006).
21. Block, A., Dhanji, H., Thompson-Tardif, S. & Floresco, S. Thalamic-prefrontal cortical-ventral striatal circuitry mediates dissociable components of strategy set shifting. *Cereb. Cortex* **17**, (2007).
22. Kato, S. *et al.* Action Selection and Flexible Switching Controlled by the Intralaminar Thalamic Neurons. *Cell Rep.* **27;22(9):2370-2382**, (2018).
23. Nakayama, H., Ibañez-Tallon, I. & Heintz, N. Cell-type specific contributions of medial prefrontal neurons to flexible behaviors. *J Neurosci.* **10.1523/JNEUROSCI.3537-17.2018**, (2018).
24. Marton, T., Seifikar, H., Luongo, F., Lee, A. & Sohal, V. Roles of Prefrontal Cortex and Mediodorsal Thalamus in Task Engagement and Behavioral Flexibility. *J Neurosci* **38(10):2569-2578**, (2018).
25. Mante, V., Sussillo, D., Shenoy, K. & Newsome, W. Context-dependent computation by recurrent dynamics in prefrontal cortex. *Nature* **7;503(7474):78-84**, (2013).
26. Rigotti, M. *et al.* The importance of mixed selectivity in complex cognitive tasks. *Nature* **497**, 585–590 (2013).
27. Hymana, J., Maa, L., Balaguer-Ballesterb, E., Durstewitzb, D. & Seamansa, J. Contextual encoding by ensembles of medial prefrontal cortex neurons. *PNAS* **109**, 5086–5091 (2012).
28. Durstewitz, D., Vittoz, N., Floresco, S. & Seamans, J. Abrupt transitions between prefrontal neural ensemble states accompany behavioral transitions during rule learning. *Neuron* **66**, 438–48 (2010).
29. Malagon-Vina, H., Ciocchi, S., Passecker, J., Dorffner, G. & Klausberger, T. Fluid network dynamics in the prefrontal cortex during multiple strategy switching. *Nat. Commun.* **9:309**, (2018).
30. Wimmer, R. *et al.* Thalamic control of sensory selection in divided attention. *Nature* **Oct 29;526(7575):705-9.**, (2015).
31. Starkweather, C., Gershman, S. & Uchida, N. The Medial Prefrontal Cortex Shapes Dopamine Reward Prediction Errors under State Uncertainty. *Neuron* **May 2;98(3):616-629.e6**, (2018).
32. Bissonette, G. & Roesch, M. Neural correlates of rules and conflict in medial prefrontal cortex during decision and feedback epochs. *Front Behav. Neurosci.* **9: 266.**, (2015).
33. Ellwood, I. *et al.* Tonic or Phasic Stimulation of Dopaminergic Projections to Prefrontal Cortex Causes Mice to Maintain or Deviate from Previously Learned Behavioral Strategies. *J Neurosci* **37(35): 8315–8329**, (2017).
34. Biró, S., Lasztóczi, B. & Klausberger, T. A Visual Two-Choice Rule-Switch Task for Head-Fixed Mice. *Front Behav. Neurosci.* **06 June**, (2019).
35. Mahn, M. *et al.* High-efficiency optogenetic silencing with somatargeted anion-conducting channelrhodopsins. *Nat. Commun.* **9:4125**, (2018).

36. Smith, M. & Kohn, A. Spatial and Temporal Scales of Neuronal Correlation in Primary Visual Cortex. *J Neurosci* **28(48): 12591–12603**, (2008).
37. Kiesel, A. *et al.* Control and Interference in Task Switching—A Review. *Psychol. Bull.* **Vol. 136, No. 5, 849–874**, (2010).
38. Rodgers, C. & DeWeese, M. Neural Correlates of Task Switching in Prefrontal Cortex and Primary Auditory Cortex in a Novel Stimulus Selection Task for Rodents. *Neuron* **82**, 1157–1170 (2014).
39. Meiron, N. & Kessler, Y. The Task Rule Congruency Effect in Task Switching Reflects Activated Long-Term Memory. *J. Exp. Psychol.* **Vol. 34, No. 1, 137–157**, (2008).
40. Collins, D., Anastasiades, P., Marlin, J. & Carter, A. Reciprocal Circuits Linking the Prefrontal Cortex with Dorsal and Ventral Thalamic Nuclei. *Neuron* **98, 366–379**, (2018).
41. Otis, J. M. *et al.* Prefrontal cortex output circuits guide reward seeking through divergent cue encoding. *Nature* **543**, 103–107 (2017).
42. Smout, C., Tang, M., Garrido, M. & Mattingley, J. Attention promotes the neural encoding of prediction errors. *PLoS Biol* **17(2): e2006812**, (2019).
43. Hauser, T., Iannaccone, R., Staempfli, P. & Drechsler, R. The Feedback-Related Negativity (FRN) revisited: New insights into the localization, meaning and network organization. *NeuroImage* **84**, (2013).
44. Garrison, J., Erdeniz, B. & Done, J. Prediction error in reinforcement learning: a meta-analysis of neuroimaging studies. *Neurosci Biobehav Rev* **Aug;37(7):1297-310**, (2013).
45. Toyomaki, A., Hashimoto, N., Kako, Y., Murohashi, H. & Kusumi, I. Neural responses to feedback information produced by self-generated or other-generated decision-making and their impairment in schizophrenia. *PLoS ONE* **2(8): e0183792**, (2017).
46. Pnevmatikakis, E. & Giovannucci, A. NoRMCorre: An online algorithm for piecewise rigid motion correction of calcium imaging data. *J. Neurosci. Methods* **Volume 291, Pages 83-94**, (2017).
47. Pnevmatikakis, E. A. *et al.* Simultaneous Denoising, Deconvolution, and Demixing of Calcium Imaging Data. *Neuron* **89**, 285–299 (2016).
48. Sheintuch, L. *et al.* Tracking the Same Neurons across Multiple Days in Ca2+ Imaging Data. *Cell Rep.* **21, 1102–1115**, (2017).